nature photonics

ARTICLES

PUBLISHED ONLINE: 20 OCTOBER 2013 | DOI: 10.1038/NPHOTON.2013.278

Light-guiding hydrogels for cell-based sensing and optogenetic synthesis *in vivo*

Myunghwan Choi[1,2], Jin Woo Choi[1,3], Seonghoon Kim[2], Sedat Nizamoglu[1], Sei Kwang Hahn[1,4] and Seok Hyun Yun[1,2†*]

Polymer hydrogels are widely used as cell scaffolds for biomedical applications. Although the biochemical and biophysical properties of hydrogels have been investigated extensively, little attention has been paid to their potential photonic functionalities. Here, we report cell-integrated polyethylene glycol-based hydrogels for *in vivo* optical-sensing and therapy applications. Hydrogel patches containing cells were implanted in awake, freely moving mice for several days and shown to offer long-term transparency, biocompatibility, cell viability and light-guiding properties (loss of <1 dB cm^{-1}). Using optogenetic, glucagon-like peptide-1 secreting cells, we conducted light-controlled therapy using the hydrogel in a mouse model with diabetes and obtained improved glucose homeostasis. Furthermore, real-time optical readout of encapsulated heat-shock-protein-coupled fluorescent reporter cells made it possible to measure the nanotoxicity of cadmium-based bare and shelled quantum dots (CdTe; CdSe/ZnS) *in vivo*.

As the autonomous building block of the body, cells have amazing abilities to sense their local environment and respond to external chemical and physical cues[1]. In addition, cells secret cytokines and hormones that are critical for homeostasis and also useful for therapeutic purposes[2]. There have been considerable efforts to use these cellular functions in medicine for diagnosis and treatment, for example, by injecting specialized cells or implanting bioengineered cells in patients[3,4]. In this cell-based approach, it is desirable, and often necessary, to communicate with these cells to receive sensor signals from them or to send regulatory control signals to them. Light offers an attractive means of communication in such biological systems. Various light-sensitive molecules and genetic engineering tools are available for building optical interfaces into cells[5,6]. Fluorescent or bioluminescent proteins can be integrated into a specific pathway of endogenous sensing machinery to achieve highly selective sensing[7]. Photoactive proteins, such as channelrhodopsin and melanopsin, can be coupled with such a pathway, leading to light-driven production of therapeutic substances where the timing and dose are controlled by light[8–11].

Despite the great promise of light-mediated, cell-based sensing and therapy, one of the fundamental challenges in this field is the high optical loss in biological tissue due to scattering and absorption[12]. In soft tissue, the 1/e optical penetration depth (L_e) at which the light intensity drops to the 1/e level (37%) is less than 1 mm for visible and near-infrared radiation[13]. Transdermal light delivery by external illumination has been shown to be viable for the optogenetic release of a therapeutic protein from cells implanted subcutaneously in mice[9]. Although this approach is feasible in small experimental animals because of their thin skin, its application to humans is unlikely to succeed because it would require high optical energy beyond the safety threshold (4 W cm^{-2}) for tissue. Endoscopes can provide minimally invasive access into the body. However, this approach limits the location of cells to near the surfaces of internal organs (such as the mucosal layer of the gastrointestinal tract) and is not suitable for continuous operation over an extended period of time (for example, several days). Another challenge in this endeavour is the need to illuminate the implanted cells and collect light from them when the cells are dispersed widely in space. Although point illumination by an optical fibre is appropriate for certain scenarios, such as focal optogenetic control in the brain[14], most applications demand a sufficient number of cells distributed over dimensions much larger than the typical 1/e optical attenuation distance (on the order of 1 mm), for which point illumination by conventional optical fibres is not suited[15].

Here, we demonstrate that hydrogels, which are commonly used as scaffolds for cell culture *in vitro* and implantation *in vivo*[16], can be designed, fabricated and used for efficient light delivery and collection, as well as cell encapsulation[17,18]. We show that cell-containing optical hydrogels can be implanted *in vivo* for an extended period, and can serve as an optical communication channel between the encapsulated cells and an external light source and detector via a strand of thin, flexible optical fibre (Fig. 1). We apply this novel approach to real-time cell-based toxicity sensing and light-controlled optogenetic production of an antidiabetic glucagon-like peptide-1 (GLP-1) in live mice.

Polymer hydrogels have been studied extensively as cellular scaffolds. The porous aqueous polymeric network of hydrogels allows small molecules, such as glucose, oxygen and secretory proteins, to be efficiently exchanged with surrounding host tissues by diffusion to facilitate the long-term survival of encapsulated cells. The cellular adhesiveness and biodegradability of hydrogels can be readily modified with chemical composition and fabrication parameters. The physicochemical, biomechanical and biological properties of hydrogels based on various synthetic or natural polymers have been characterized, and numerous recipes to optimize these properties have been established[19,20]. However, relatively little research has been conducted in relation to the optimization of

[1]Harvard Medical School and Wellman Center for Photomedicine, Massachusetts General Hospital, 50 Blossom Street, Boston, Massachusetts 02114, USA, [2]WCU Graduate School of Nanoscience and Technology, Korea Advanced Institute of Science and Technology, 373-1 Guseong-dong, Yuseong-gu, Daejeon, Korea, [3]Wonkwang Institute of Interfused Biomedical Science, Department of Pharmacology, School of Dentistry, Wonkwang University, Seoul, Korea, [4]Department of Materials Science and Engineering, Pohang University of Science and Technology, 77 Cheongam-Ro, Nam-Gu, Pohang, Korea; †Present address: Harvard University, 65 Lansdowne Street, UP-525, Cambridge, Massachusetts 02139, USA. *e-mail: syun@hms.harvard.edu

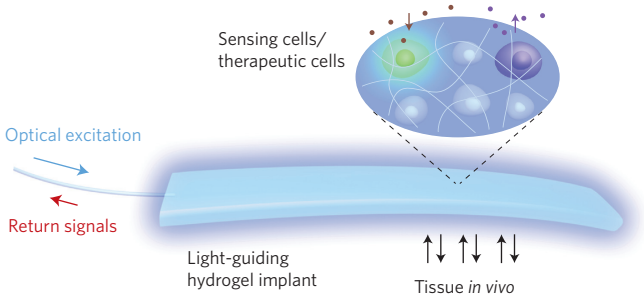

Figure 1 | Schematic of a light-guiding hydrogel encapsulating cells for *in vivo* sensing and therapy. The cells in the implanted hydrogel produce luminescence in response to environmental stimuli (sensing) and secrete cytokines and hormones following photo-activation (therapy). The light-guiding hydrogel establishes bidirectional optical communication with the cells, allowing real-time interrogation and control of the biological system *in vivo*.

their optical properties. In the present study, we chose polyethylene glycol (PEG)-based hydrogels, widely used for various biomedical applications[21]. We began our study by determining the optimal design parameters, including molecular weight, water content and shape of the hydrogels, so as to achieve the desired functional properties. PEG-based hydrogels were formed by ultraviolet-induced polymerization and crosslinking of PEG diacrylate (PEGDA) precursor solutions mixed with photoninitators (Irgacure, 0.05% wt vol^{-1}).

Optical transparency of PEG hydrogels

It is necessary to be able to control the transparency of hydrogels for photonic applications. To determine the optimal compositions of the hydrogels we measured optical loss spectra for hydrogels prepared using PEGDA of various molecular weights (0.5, 2, 5 and 10 kDa), but at the same concentration (10% wt vol^{-1}) (Fig. 2a). PEG hydrogels with a molecular weight of 0.5 kDa in standard 1 cm cuvettes were white opaque, indicating strong uniform scattering across the visible spectrum. With increasing molecular weight, the PEG hydrogels became transparent. Attenuation spectroscopy confirmed the strong dependency on molecular weight of the precursor polymer. PEG hydrogels of 0.5 kDa had an optical loss of ~25 dB cm^{-1} (that is, $L_e = 1.8$ mm) in the visible range (400–700 nm) (Fig. 2b). When the PEGDA concentration increased to 60% wt vol^{-1} or higher, the hydrogels became noticeably more transparent (Supplementary Fig. S1). However, these concentrations were not adequate for cell encapsulation because of the low water content (<90%). Furthermore, the hydrogels became increasingly stiffer with concentration, which can reduce cell viability and cause undesirable tissue damage when implanted *in vivo*. Hydrogels prepared with 2, 5 and 10 kDa PEGDA exhibited much lower optical loss. In the blue to green range of 450–550 nm, the average loss was measured to be 0.68 dB cm^{-1} ($L_e = 6.4$ cm) for 2 kDa, 0.23 dB cm^{-1} ($L_e = 19$ cm) for 5 kDa and 0.17 dB cm^{-1} ($L_e = 26$ cm) for 10 kDa PEGDA. Hydrogels were fabricated in rectangular custom-made glass moulds by *in situ* photo-induced crosslinking (Supplementary Fig. S2). The typical dimensions of the PEG hydrogels were 4 mm (width) × 1 mm (height) × 10–40 mm (length). The fabricated 0.5 kDa hydrogels (10% wt vol^{-1}) were semi-opaque as seen through the 1 mm thickness, whereas the 5 kDa hydrogels were markedly more transparent (Fig. 2c).

Effects of swelling on physical properties

To investigate the stability of the optical properties of the hydrogels in an aqueous environment we performed a swelling test. The hydrogels were immersed in phosphate buffered saline (PBS) for 12 h, and the fractional weight increase due to water absorption was measured[22]. The swelling ratio increased with the PEGDA molecular weight increasing from 0.5 to 10 kDa (Fig. 2d). The rectangular shape of the 10 kDa hydrogels was found to be severely deformed due to swelling, whereas 0.5–5 kDa hydrogels maintained their rectangular shapes with minimal distortion. Interestingly, despite the swelling, all the hydrogels (0.5–10 kDa) showed no apparent changes in transparency. We also found that hydrogels became more flexible with increasing molecular weight. Although 0.5 kDa hydrogels were quite brittle, 5 kDa hydrogels were highly elastic and could easily be bent and twisted (Fig. 2e). In view of their excellent transparency, structural stability and mechanical flexibility, we chose to use PEG hydrogels with 5 kDa molecular weight and 10% wt vol^{-1} concentration in the following studies.

Light guiding in slab hydrogels

We investigated the optical-guiding properties of rectangular slab hydrogels with dimensions of 4 mm (width) × 1 mm (height) × 40 mm (length). The refractive index of 10% wt vol^{-1} hydrogels was estimated to be ~1.35 (the index of 100% PEG is 1.465). When a laser beam (491 nm) was launched into the hydrogel at an angle, it propagated in a zigzag path (Fig. 2f) due to total internal reflection (TIR) at the hydrogel–air interface. To provide a fibre-optic connection, a multimode fibre (core diameter, 100 μm; numerical aperture, 0.37) was integrated during fabrication of the hydrogels (Supplementary Fig. S2). Light from an external light source was coupled into the hydrogel via an optical-fibre pigtail (Fig. 3a). Light from the optical fibre was dispersed in the cross-section of the hydrogel nearly uniformly after a several-millimetre-long diffraction region (Fig. 3b). The light propagated all the way to the distal end of the 4-cm-long hydrogel waveguide and exited through the end surface (Fig. 3b).

Light collection by hydrogels

We also tested the ability of the hydrogel waveguide to collect light generated from the hydrogel or from the surrounding tissue and then deliver it to a photodetector. We measured the amount of fluorescence light collected from a green fluorescent plate or dye solution (FITC; 5% wt vol^{-1}) over varying distances, with and without a hydrogel lying between the sample and the fibre (Fig. 3c). Excitation light (455 mm) was delivered from a laser through the pigtail fibres. The length of the hydrogel was varied by cutting it from 40 mm to 30, 20, 10 and 5 mm (length L). The collection efficiency of the optical fibre alone decreased with $1/L^2$, as expected from its geometry. However, with hydrogel, the collection efficiency followed a linear decay function according to $1/L$ (Fig. 3d). The difference in ratio, or the enhancement factor, increased linearly with the length of the hydrogel, and was about 80-fold (19 dB) for 4-cm-long hydrogels (Fig. 3e). Taken together, our results demonstrate the desirable optical functions of the hydrogel, both in terms of transmitting light from an external source to the inside of the hydrogel and for delivering light from the hydrogel to an external detector.

Cell-encapsulated hydrogels

For cell encapsulation, Hela (human cervical cancer cell line) cells were mixed into the precursor PEGDA solution with Arg–Gly–Asp (RGD) peptides (1 mM), before crosslinking. Because of their refractive index profile (1.35–1.36 in the nucleus and 1.36–1.39 in the cytoplasm[23]), the cells in the hydrogel refract and scatter light. Absorption spectroscopy was applied to show the scattering-induced loss of cell-encapsulated hydrogels (Fig. 3f). For a given cell density, the attenuation was relatively uniform over the visible to near-infrared range (400–900 nm), with slight decreases with wavelength. The attenuation coefficients were found to increase nonlinearly with cell density (Fig. 3g), reaching as high as

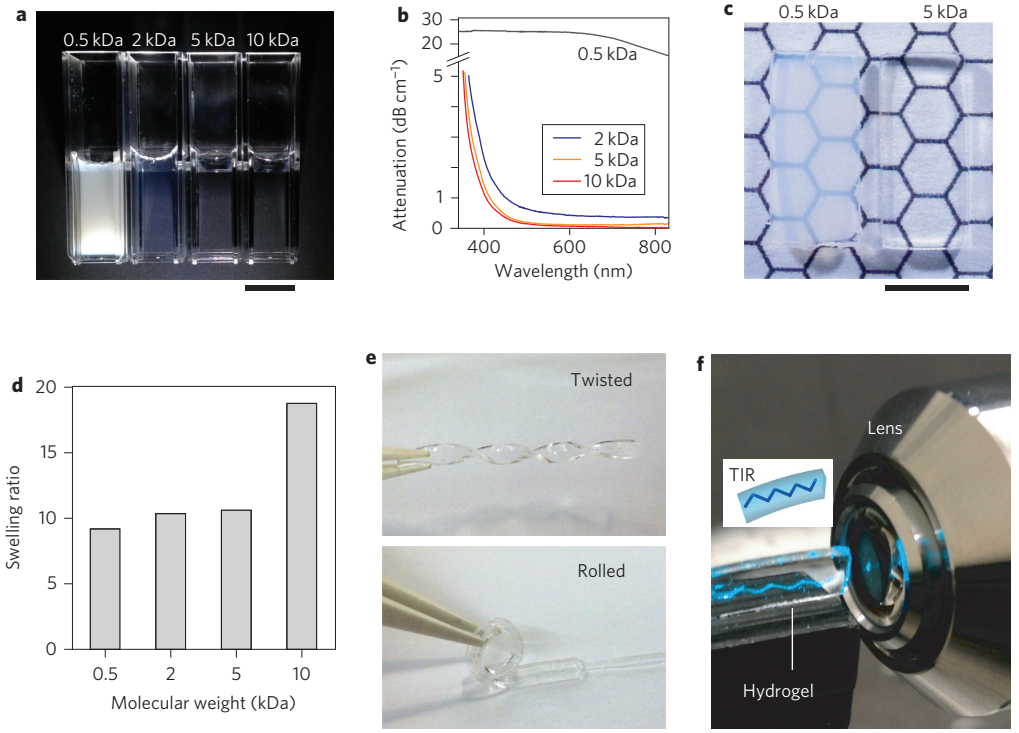

Figure 2 | Characteristics of hydrogels. a, Photograph of PEG-based hydrogels prepared using 10% wt vol^{-1} PEGDA solution with PEGDA molecular weights of 0.5, 2, 5 and 10 kDa. Scale bar, 1 cm. **b**, Optical attenuation spectra of PEG hydrogels prepared with different molecular weights of PEGDA. **c**, Rectangular 0.5 and 5 kDa hydrogels (thickness, 1 mm). Scale bar, 5 mm. **d**, Swelling ratios of PEG hydrogels. The swelling ratio was calculated by dividing the weight of swollen hydrogel by the weight of dried hydrogel ($n = 3$). **e**, Mechanical flexibility of the PEG hydrogel (5 kDa, 10%). **f**, Demonstration of TIR within the slab hydrogel.

2.4 dB cm^{-1} ($L_e = 1.8$ cm) with 5×10^6 cells ml^{-1} in the wavelength range 450–500 nm. The cell density of $\sim 1 \times 10^6$ cells ml^{-1} was determined to be optimal for 4-cm-long hydrogels, for which the loss is less than 1 dB cm^{-1} and the 1/e attenuation length ($L_e = 5.6$ cm) is comparable to the length of the hydrogel. At this cell density, a hydrogel with dimensions of $1 \times 4 \times 40$ mm^3 (0.16 cm^3) could contain up to 160,000 cells and, without molecular absorption, carry 70% of the light to its distal end.

Implantation of cell-containing hydrogel *in vivo*

Cell-containing hydrogels were implanted into a subcutaneous pocket in mice through a 1-cm-long skin incision on the back (Fig. 4a). The pigtail fibre was securely cemented onto the skull to establish stable light coupling to the hydrogel while the animal was awake and moving freely (Fig. 4b; Supplementary Movie S1). Light leaking out of the hydrogel to the surrounding tissue could be readily monitored through the thin skin layer (Fig. 4c). The optical intensity throughout the entire implant varied by no more than 6 dB, which is slightly higher than the 1 dB cm^{-1} measured in air and is due to the contact with the tissue (index, 1.34–1.41; Fig. 4d). By comparison, when only a multimode fibre was implanted without hydrogel, the 1/e light intensity was constrained to a small region with a diameter of 2–3 mm as seen through the skin (Fig. 4c,d). This result represents a 40-fold increase of the illumination area with the light-guiding scaffold.

The hydrogels and surrounding tissues were harvested at days 3 and 8 after implantation ($n = 3$). Fluorescence microscopy with cell viability probes showed that ~80% of the embedded cells were found live in the hydrogels *in vitro* after photo-crosslinking, and more than 70% and 65% of the embedded cells in the implanted hydrogels remained viable after 3 and 8 days, respectively (Fig. 4e), which was consistent with measurements with hydrogels in a culture dish *in vitro* (Fig. 4f, Supplementary Fig. S3). The decreases in optical transmittance at 3 and 8 days *in vitro* and *in vivo* were less than 1 dB cm^{-1} (Fig. 4g). Histology suggested there were no major immune-cell infiltrations, but the formation of connective tissues around the implants, which is a typical mild reaction to foreign bodies, was observed in all, but not in sham-surgery, animals (Fig. 4h). The newly formed tissues were moderately vascularized. The hydrogel implants as a whole came off the surrounding tissues easily during tissue collection, indicating a lack of adhesion between the tissues and hydrogels.

In vivo sensing of nanotoxicity

We applied fibre-optic cell-containing hydrogel implants for the measurement of the toxicity of quantum dots *in vivo*. To sense cellular toxicity we used an intrinsic cellular cytotoxicity sensor—heat-shock-protein 70 (hsp70)[24]—which is activated when cells are under cytotoxic stress, such as from heavy metal ions and reactive oxygen species, and green fluorescent protein (GFP) under the hsp70 promoter. Cadmium is a widely used heavy metal in quantum dots, but can cause cytotoxic effects when released as a result of degradation of the quantum dots. The magnitude of green fluorescence from these sensor cells *in vitro* increased with a sublethal dose of $CdCl_2$ up to 1 μM, but saturated at higher concentrations of 1–5 μM (Supplementary Fig. S4). Two types of cadmium-containing quantum dots were tested: core-only CdTe and core/shell CdSe/ZnS nanoparticles. The sizes of the bare and shelled quantum dots were ~3.2 and 5.2 nm, respectively, so they emit red fluorescence (605 nm), which is readily distinguishable from the green fluorescence signal. When the cells were encapsulated in a hydrogel *in vitro*, the sensor signal increased with the concentration of CdTe quantum dots in the medium, but no noticeable change of green fluorescence was observed when CdSe/ZnS quantum dots were used (Fig. 5a,b). This result confirmed the dramatic role of the ZnS shell in reducing cellular toxicity.

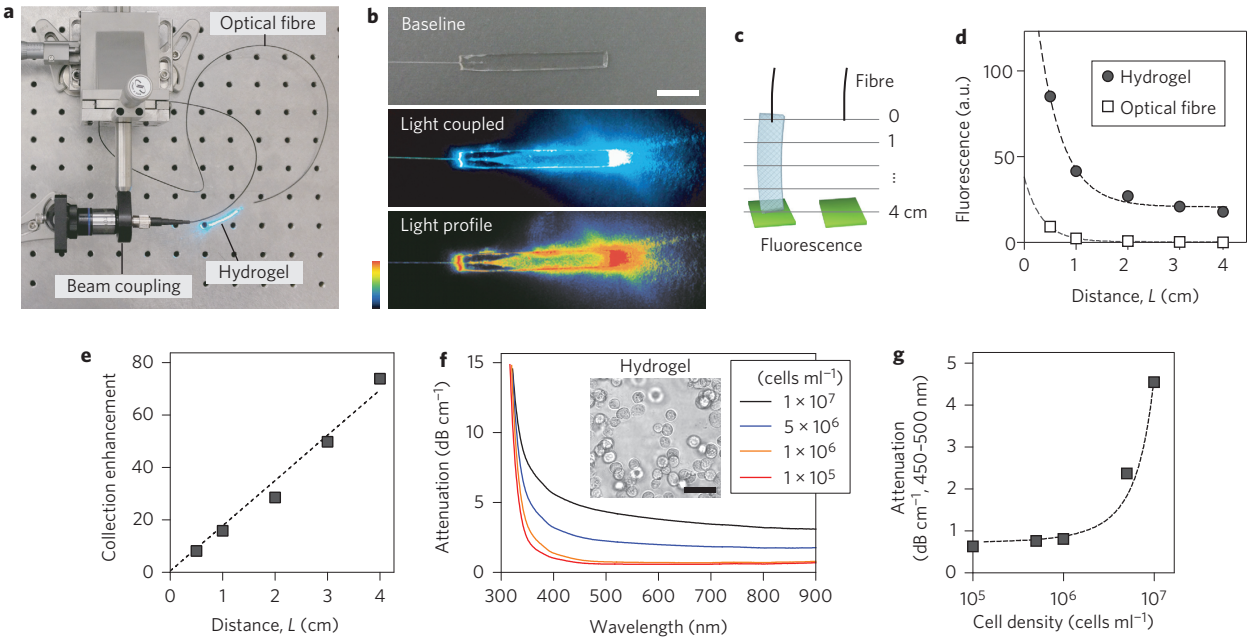

Figure 3 | Light-guiding properties of fibre-optic hydrogels. a, Set-up for coupling light into a hydrogel waveguide via a multimode fibre. **b**, Photographs showing light coupling to a hydrogel. Top: hydrogel before light coupling; middle: hydrogel after light coupling; bottom: pseudo-colour image of the spatial profile of the scattered light. **c**, Schematic of set-up for measuring collection efficiency. A fluorescent sample (green) was placed in contact with hydrogels of varying lengths (left) or at equivalent distances from a multimode fibre (right). **d**, Magnitude of fluorescence collected by the optical fibres with and without hydrogel. Dashed lines, curve fits with $1/L^2$ and $1/L$ dependencies for the hydrogel and optical fibre alone, respectively. **e**, Ratio of fluorescence with and without hydrogels. Dashed line represents the linear regression ($R^2 = 0.98$). **f**, Optical attenuation spectra of hydrogels at various cellular density levels. Inset: phase-contrast micrograph of the hydrogel. Scale bar, 50 μm. **g**, Average optical attenuation of a hydrogel with 1×10^6 cells cm^{-3} in the spectral range 450–500 nm. Dashed line shows exponential fit ($R^2 = 0.96$).

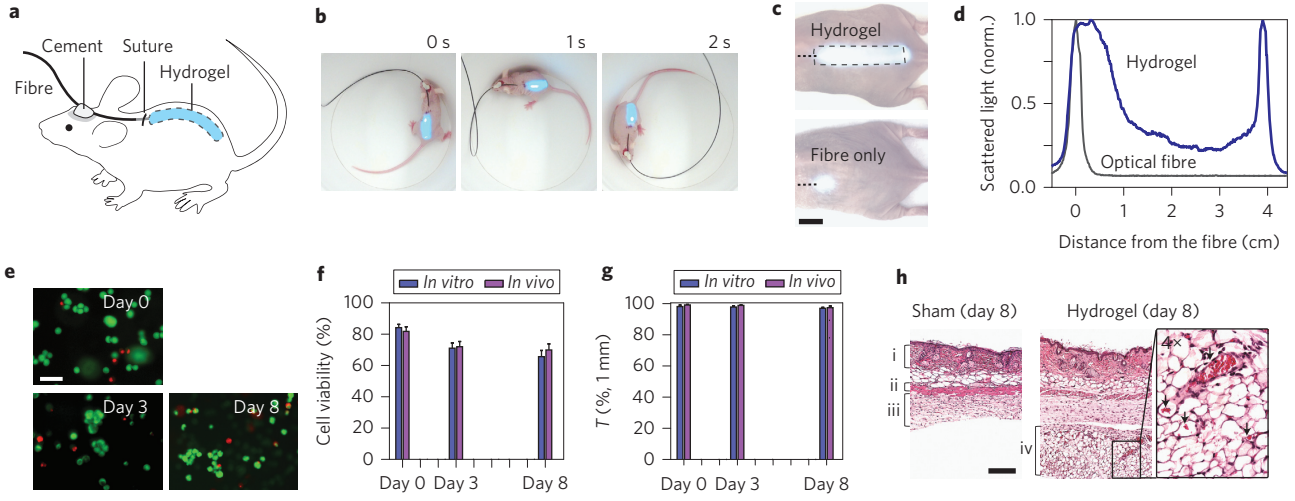

Figure 4 | Hydrogel implants *in vivo*. a, Schematic of a fibre-pigtailed hydrogel waveguide implanted in a mouse. **b**, A hydrogel-implanted mouse in a freely moving state. Blue light (491 nm) was coupled. **c**, Photographs showing the light-scattering profiles from an optical hydrogel implant (top) and from an optical fibre only (bottom). **d**, Axial profiles of the magnitude of scattered light from the hydrogel implant (blue) and optical fibre only (black). **e**, Fluorescence images of hydrogel implants immediately after taken out of mice at 3 and 8 days following implantation in comparison to control (day 0; before implantation). Live cells emit green fluorescence from a membrane-permeable live cell-staining dye (calcein-AM), and dead cells are identified by red fluorescence from ethidium bromide in the cell nuclei. Scale bar, 50 μm. **f**, Long-term viability of encapsulated cells *in vivo*. Error bars are standard deviations ($n = 6$ each). **g**, Change in optical transmittance of the hydrogel implants *in vivo*. **h**, H&E histology images of skin tissues examined 8 days after implantation: (i) dermis, (ii) panniculus carnosus, (iii) subcutaneous loose connective tissue layer and (iv) newly formed connective tissue layer. In the magnified image (right), arrows indicate red blood cells in blood vessels. Scale bar, 100 μm.

We next implanted cell-encapsulating hydrogels into three groups of mice, which were treated by a systemic injection of CdTe quantum dots (100 pM), CdSe/ZnS quantum dots (100 pM) and PBS only. Time-lapse fibre-optic fluorescence measurement (Supplementary Fig. S5) showed a significant increase in green fluorescence in the CdTe-treated group, but not in the

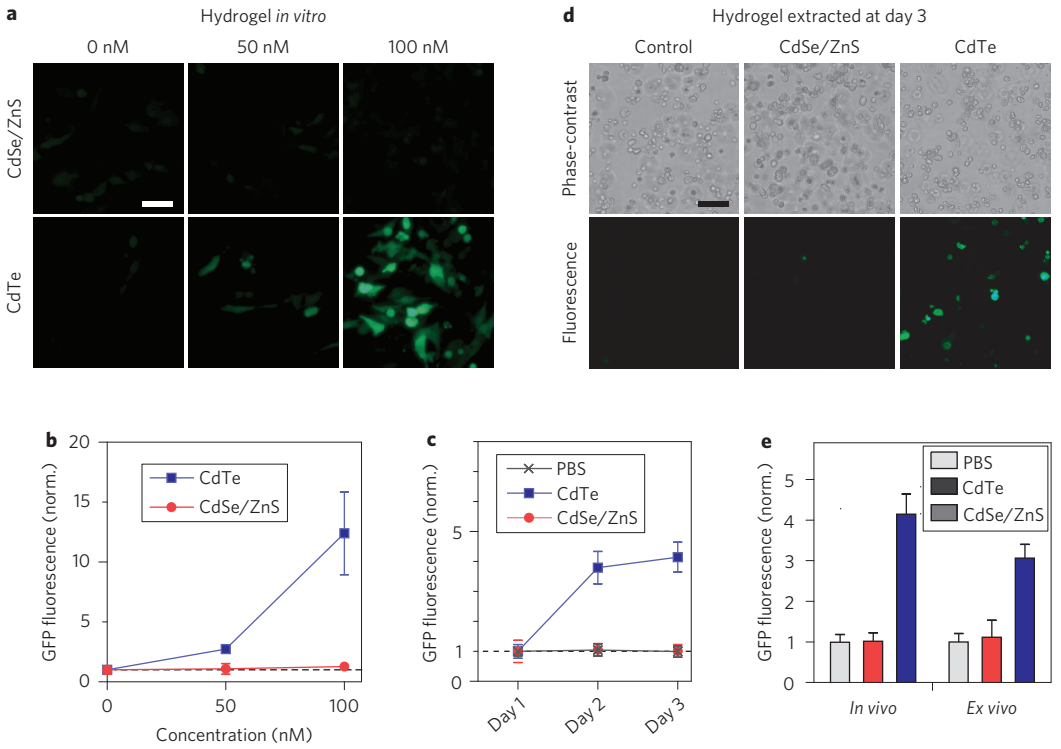

Figure 5 | Cell-based sensing of nanocytotoxicity of quantum dots. a, Fluorescence images of sensor cells in hydrogels *in vitro*, two days after adding CdTe (bottom) or CdSe/ZnS (top) quantum dots into the medium. Scale bar, 20 μm. **b**, Magnitude of green fluorescence from the hydrogels, measured through the pigtail fibres. **c**, *In vivo* measurement of fluorescence signals from the sensing cells in hydrogels implanted in live mice. Quantum dots were administered by intravenous injection 24 h after the hydrogels were implanted. **d**, Fluorescence images of hydrogels extracted from the mouse at day 3. Scale bar, 20 μm. **e**, Comparison of GFP fluorescence measured fibre-optically *in vivo* (left) and by fluorescence microscopy *ex vivo* (right).

CdSe/ZnS-treated and control groups, at days 1 and 2 after treatment (Fig. 5c). To validate this measurement, we extracted the hydrogel implants from the mice at day 2 and examined them with fluorescence microscopy (Fig. 5d). The total magnitude of GFP fluorescence from the cells was qualitatively consistent with the values measured *in situ* in live mice (Fig. 5e). These results represent the first real-time measurement of systemic cellular toxicity by cadmium-based quantum dots and the effect of surface capping by biocompatible shells.

Optogenetic therapy of diabetic mice

To demonstrate cell-based therapy we used a vector construct previously developed for optogenetic synthesis of GLP-1[9] and generated a stably transfected cell line (Supplementary Fig. S6). Following absorption of blue light, the light-responsive protein melanopsin is activated in the plasma membrane, which increases intracellular calcium and consequently activates a transcription factor (nuclear factor of activated T cell, NFAT), which drives the production of GLP-1. GLP-1 is an antidiabetic secretory protein that promotes glucose homeostasis by stimulating glucose-dependent insulin secretion[25]. We first confirmed the intended function of these optogenetic cells when encapsulated in a hydrogel *in vitro*. To monitor the change in the intracellular calcium level, the optogenetic cells were loaded with a fluorescence-based calcium indicator (OGB1-AM). More than 80% of the cells illuminated by blue light showed an increase of intracellular calcium within several seconds (Fig. 6a,b). We performed enzyme-linked-immunosorbent assay (ELISA) on the media in which the cell-encapsulated hydrogels were immersed and measured a significant increase of GLP-1 concentration in the light-exposed (on) samples compared to non-illuminated (off) controls (Fig. 6c). This result confirmed the optogenetic synthesis of GLP-1 and the permeability of secreted GLP-1 molecules through the crosslinked hydrogel.

To investigate the therapeutic potential of the optogenetic system, we implanted cell-containing hydrogel into chemically induced diabetic mice[26]. Blue light (455 nm, 1 mW) was fibre-optically delivered for 12 h after implantation. At 48 h after implantation, light-exposed animals ($n = 4$) showed an approximately twofold increase in the blood GLP-1 level compared to the non-illuminated control group (Fig. 6d). To validate physiological efficacy we performed a glucose tolerance test. Following an intraperitoneal injection of glucose (1.5 g kg^{-1}), the light-treated group achieved significantly improved glucose homeostasis, with the blood glucose level returning to the initial level of 14 mM in 90 min (Fig. 6e). In contrast, the blood glucose level of the non-treated group remained higher than 28 mM, even after 120 min (Fig. 6e). This result demonstrates the therapeutic potential of the cell–hydrogel implant for optically controlled optogenetic synthesis in the body.

Discussion

Recently, there has been growing interest in developing photonics devices based on biomaterials such as silk fibroin[27], agar[17] and synthetic polymers[28]. Various biocompatible photonic components, such as optical fibres and gratings, have been demonstrated, and their optical functions have been tested in *in vitro* and, to some extent, *in vivo* settings. In this study, we used PEG-based hydrogels to demonstrate, for the first time, *in vivo* biomedical applications of cell-containing optical waveguides. We have shown that hydrogels can serve not only as a cellular scaffold but also as a bidirectional optical communication channel for encapsulated cells. Optical hydrogel implants encapsulating cells with luminescent reporters and optogenetic gene-expression machinery allowed us to perform

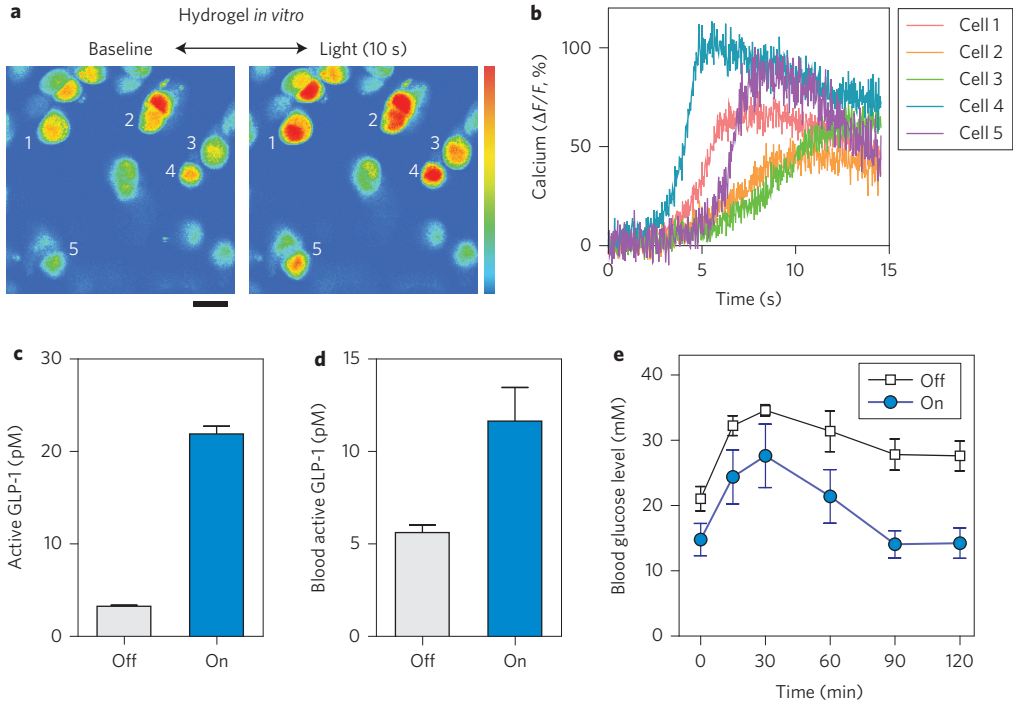

Figure 6 | Optogenetic therapy in a mouse model of diabetes. a, Fluorescence calcium-level imaging of optogenetic cells in a hydrogel waveguide *in vitro*. Upon delivering blue light (455 nm) through the fibre for 10 s at 1 mW, fluorescence from an intracellular calcium indicator (OGB1-AM) increased significantly. Scale bar, 20 μm. **b**, Time traces of intracellular calcium signals from various cells (indicated in **a**). **c**, Concentrations of active GLP-1 in the medium of hydrogels with (on) and without (off) activation light. **d**, Level of GLP-1 in blood plasma measured *in vivo* at 2 days after light exposure. **e**, Blood glucose levels in chemically induced diabetic mice with and without activation light. Error bars, standard deviations ($n = 4$).

the first real-time sensing of nanotoxicity in animals and also optogenetic diabetic therapy with an optical power of only 1 mW, which is much more efficient than conventional transdermal delivery[9].

Optical transparency is essential for most photonic applications of hydrogels. We found that the longer PEGDA polymers yielded a higher transparency after crosslinking. This general tendency may be explained by the formation of pores in crosslinked hydrogels. In solutions before crosslinking, the precursor PEG chains are homogeneously dispersed in water and, therefore, transparent. Ultraviolet-induced polymerization reorganizes the monomer distribution following energy minimization. This can introduce spatial inhomogeneity depending on the molecular compositions and crosslinking parameters. As a distinct phenomenon, phase separation between the polymer-rich phase and the water-rich phase[29] can occur when the water content exceeds the maximum equilibrium level the crosslinked polymer can take up during polymerization. The resulting pores, with sizes ranging from nanometres to micrometres, cause light scattering due to the refractive index contrast, and reduce transparency. This mechanism explains the opaqueness of 0.5 kDa PEG hydrogels made at 10% wt vol^{-1} and the improved transparency at lower water contents (higher concentrations >15% wt vol^{-1}) (Supplementary Fig. S2).

The light-guiding properties of hydrogels can be tailored for specific requirements by controlling the shape and structure of the hydrogels. For example, cell-based therapy in patients would require a sizable hydrogel containing a large number of cells so as to produce a physiologically relevant dose. In this case, an additional cladding layer with a lower refractive index may be used to enhance guiding. The width of the hydrogel may be tapered to compensate for cell-induced optical loss and thereby obtain a more uniform optical intensity throughout the entire volume. Besides PEG, other polymers widely used in cell culture and tissue engineering, such as hyaluronic acid, alginate and collagen, are good candidates for optical hydrogels. Hydrogels based on these polymers have shown excellent properties for cell encapsulation. Compositional screening and optimization for optical characteristics could result in a range of material options for light-guiding hydrogels with different refractive indices. Other than a preformed hydrogel, injectable hydrogels such as thermo-responsive gels may be used to facilitate minimally invasive implantation via *in situ* gelation[30]. Further optimization of mechanical stability, flexibility or biodegradation is also achievable by modifying the chemical compositions or fabrication protocol[31]. Additionally, a photodegradable group may be introduced to control biodegradation kinetics.

There remain challenges for the clinical application of hydrogels[32]. First, as the amount of therapeutic substances required for systemic diseases is proportional to bodyweight, larger hydrogels are required. Our data indicate that it is plausible to increase the cell density fivefold (5×10^6 cells cm^{-3}) without lowering the optical transmission substantially, and even higher concentrations may be possible with optimized hydrogel designs. Furthermore, different host cells with enhanced transfection efficiency may be used. For example, HEK293 cells have an order-of-magnitude higher protein production rate than the Hela cells used in our work[9]. Additionally, genetic and protein engineering to increase the production rate and stability of therapeutic proteins will allow a further reduction in implant size[33]. Second, the cell-hydrogel implant should be functionally stable *in vivo* for several weeks and months depending on the application (for example, for chronic problems). Such a long lifetime is currently challenging, although not unattainable[34]. Finally, more careful investigation of the long-term host response against implanted hydrogels is required[35]. All the above issues have long been major research topics in the fields of regenerative medicine and tissue engineering. Continuing progress in this field will increase the clinical potential of the hydrogel-based technique[21].

The light-guiding hydrogel system can also make use of non-cell-based chemical sensors and photoactive therapeutic molecules[36]. Although this approach does not benefit from the unique features, such as self-sustainability, of cells, it provides simplicity and allows existing molecular probes and drugs to be used in conjunction with light-guiding hydrogels.

In conclusion, we have demonstrated a new optical hydrogel waveguide that offers excellent low-loss light-guiding properties and simultaneously meets all practical requirements, including long-term cell encapsulation, mechanical flexibility and long-term transparency *in vivo*. By coupling the numerous cellular sensing and secretary protein-production pathways with optical readout and optogenetic signalling, the optical hydrogel system has the potential to be a platform technology with a broad range of applications in diagnosis and therapy.

Methods

Hydrogel fabrication. PEGDA (Laysan Bio) solution in PBS at concentrations between 10 and 60% wt vol^{-1} was mixed with 0.05% wt vol^{-1} photoinitiator Irgacure 2959 (Ciba)[22]. The solution was transferred to a custom-made glass mould and exposed to an ultraviolet lamp (365 nm, 5 mW cm^{-2}; Spectroline) for 15 min. For fibre coupling, a multimode optical fibre (100 μm core, 0.37 NA; Doric Lenses) was embedded in the polymer solution at its tip (a few millimetres) and aligned to the long axis of the hydrogel before photo-crosslinking. Epoxy was applied to reinforce the fibre–hydrogel joint. For cell encapsulation, cells in a culture dish were treated with trypsin, quantified, and mixed into the PEGDA solution at a concentration of 5×10^5 to 1×10^6 cells ml^{-1} before photo-crosslinking. The high cell viability of this protocol was confirmed with multiple cell lines including Hela (human cervical cancer cell), HEK293T (human kidney cell) and EL4 (mouse T cell) (Supplementary Fig. S3). The crosslinked hydrogel was placed in culture medium and incubated for more than one day before implantation into a mouse. The cell medium was replaced at 1 h, 3 h and every 24 h.

Preparation of cells. Hela cells (ATCC) were maintained in Dulbecco's modified Eagle's medium (DMEM) supplemented with 10% fetal bovine serum and 1% antibiotics at 37 °C in 5% CO_2. For cytotoxicity reporter cells, Hela cells were transiently transfected with an HSP70-GFP vector using Lipofectamine 2000 (Life Technologies) according to the manufacturer's protocol. After incubation overnight, the cells were trypsinized and encapsulated in a hydrogel for the sensing experiments. An optogenetic cell line was generated by stable transfection of two vectors, namely pHY42 (human melanopsin; neomycin resistant) and pHY57 (NFAT-shGLP1, NFAT-driven short-variant human GLP1; hygromycin resistant). Hygromycin (150 mg ml^{-1}) and G418 (800 μg ml^{-1}) were added every other day from 48 h after introduction of the vectors, for 2 weeks. Selected colonies were transferred into a 24-well plate and incubated. After being confluent, the cells dissolved in RIPA buffer containing 1% Triton-X100 and 0.1% SDS. The lysates were separated by a 10% SDS-polyacrylamide gel electrophoresis (PAGE) gel and transferred to a polyvinylidene difluoride (PVDF) membrane. To check the expression level of melanopsin, the membrane was tested by western blot using polyclonal antibody against human melanopsin (ab65641, Abcam). Expression of shGLP-1 was confirmed by a GLP-1 enzyme-linked immunosorbent assay kit (Millipore). Cell lines that highly express both melanopsin and shGLP-1 were used for optogenetic experiments.

Characterization of hydrogels. PEG hydrogels were prepared in standard 1-cm-wide poly(methyl methacrylate) disposable cuvettes, and optical attenuation was measured using a scanning spectrophotometer (Thermo Scientific). The optical transmittance of slab hydrogels was measured through their 1-mm-thick axes using the collimated beam from a blue continuous-wave laser (20 mW, $\lambda = 491$ nm; Cobolt Calypso, Cobolt) and an optical power meter (1918-R, Newport). Swelling ratios, defined as the weight of dried hydrogel divided by the weight of hydrogel, were measured after placing hydrogels in PBS for 12 h (ref. 22). For the cell viability test, a hydrogel was washed in serum-free medium and incubated in serum-free medium containing calcein AM (1 μl ml^{-1}; Life Technologies) and ethidium bromide (2 μl ml^{-1}; Life Technologies) for 30 min. The hydrogel was then incubated in serum-free medium for 15 min, washed with PBS, and imaged with a fluorescence microscope (Olympus).

Implantation. After anaesthetizing a mouse by intraperitoneal injection of ketamine (100 mg kg^{-1}) and xylazine (10 mg kg^{-1}), the dorsal skin was incised over ~1 cm horizontally, and a round spatula was inserted to form a subcutaneous pocket and then pulled out. The hydrogel was placed on the spatula and they were inserted together into the subcutaneous pocket. The spatula was slowly retracted, while the hydrogel remained inside. The incised skin was sutured using a 6–0 nylon suture. For the fibre-connected hydrogel waveguide, a part of the scalp was incised and periosteum was retracted gently using Kimwipes. The optical fibre was fixed on the exposed skull with a drop of dental cement (GC Fuji I, GC America).

Histology. A sample of full-thickness skin around the hydrogel implant was excised and fixed in 4% formalin for 48 h or longer. The skin sample was frozen-sectioned at a thickness of 5 μm and stained with haematoxylin and eosin (H&E). The slide was imaged with a bright-field microscope (Olympus) with a ×10 objective lens.

Optical set-up. A fibre-coupled light-emitting diode (LED; $\lambda = 455$ nm; M455F1, Thorlabs) was coupled to a hydrogel through a fluorescence detection cube with a dichroic cutoff at 500 nm (Doric lenses), and emission was measured using a spectrometer (Andor). For optogenetic stimulation, the output of the fibre-coupled LED was modulated to 0.1 Hz rectangular pulses with 50% duty cycle (5 s on followed by 5 s off) using a function generator. Optogenetic cells in culture were illuminated at an intensity of 0.5 mW cm^{-2} for 12 h. To illuminate cells in the hydrogel waveguide implant, an average optical power of 1 mW was coupled into the pigtail fibre for 12 h.

Preparation of quantum dots. CdTe quantum dots were synthesized in house using a hydrothermal route by reacting Cd^{2+} with NaHTe solution[37]. To obtain Cd^{2+} solution, 2.35 mM of $Cd(ClO_4)_2{\cdot}6H_2O$ (Sigma) was dissolved in 125 ml of distilled water, mixed with 5.7 mM of thioglycolic acid (Sigma) and adjusted to a pH of 11.6. For NaHTe solution, 1.2 mM of Te powder and 6 mM of $NaBH_4$ (Sigma) were reacted in a three-necked flask by adding 5 ml of N_2-saturated distilled water. The flask was heated to 60 °C under nitrogen gas purging until the solution turned white. The prepared solutions were mixed to form CdTe precursor solution. The precursor solution was heated to 100 °C until its fluorescence emission reached 600 nm, and the solvent was then exchanged for PBS through isopropanol precipitation. CdSe/ZnS quantum dots with amphiphilic coatings were purchased from Life Technologies (Qdot-605, Q21301MP).

Cytotoxicity sensing. For the *in vitro* study, cytotoxicity reporter cells were treated with CdSe/ZnS or CdTe one day after transfection. The change in GFP expression was measured 24 h after treatment. For the animal study, cell-encapsulating hydrogels were implanted into 8-week-old BALB/c nude mice. One day after implantation, the baseline fluorescence from the implant was measured fibre-optically. Different groups of mice received intraperitoneal injections of PBS (100 μl), CdSe/ZnS quantum dots (100 μl of 1 μM in PBS) and CdTe quantum dots (100 μl of 1 μM in PBS), respectively. The fluorescence levels were measured one and two days after the injection.

Glucose tolerance test. To test the therapeutic efficacy of optogenetically secreted GLP-1, we used a chemically induced diabetes model prepared by the administration of low-dose streptozotocin[26]. Briefly, 8-week-old BALB/c nude mice were prestarved for 4 h and received streptozotocin (40 mg kg^{-1}) diluted in 0.1 M citrate buffer (pH 4.5) for five consecutive days. For six days, 10% sucrose solution was provided in drinking water to prevent hypoglycaemia. After 2 weeks, blood glucose level was measured using a digital glucose meter (Fora), and a blood glucose level higher than 250 mg dl^{-1} was considered a diabetic condition. For the glucose tolerance test, mice were starved for 6 h and baseline glucose levels were measured. After administrating 1.5 g kg^{-1} of glucose intraperitoneally, blood glucose levels were measured by titration at 15, 30, 60, 90 and 120 min after glucose injection. All animal experiments were performed in compliance with institutional guidelines and approved by the subcommittee on research animal care at the Massachusetts General Hospital.

Data analysis. ImageJ was used for image processing and data quantification. Data were expressed as the means ± standard error of the mean. Statistical analyses were performed using Graph Pad Prism software. Statistical differences were analysed by *t*-test where indicated. *P*-values of less than 0.05 were considered to be statistically significant.

Received 20 April 2013; accepted 13 September 2013; published online 20 October 2013

References

1. Miller-Jensen, K., Janes, K. A., Brugge, J. S. & Lauffenburger, D. A. Common effector processing mediates cell-specific responses to stimuli. *Nature* **448,** 604–608 (2007).
2. Pancrazio, J. J., Whelan, J. P., Borkholder, D. A., Ma, W. & Stenger, D. A. Development and application of cell-based biosensors. *Ann. Biomed. Eng.* **27,** 697–711 (1999).
3. Banerjee, P. & Bhunia, A. K. Mammalian cell-based biosensors for pathogens and toxins. *Trends Biotechnol.* **27,** 179–188 (2009).
4. El-Ali, J., Sorger, P. K. & Jensen, K. F. Cells on chips. *Nature* **442,** 403–411 (2006).
5. Zhang, F. *et al.* Optogenetic interrogation of neural circuits: technology for probing mammalian brain structures. *Nature Protoc.* **5,** 439–456 (2010).
6. Giepmans, B. N., Adams, S. R., Ellisman, M. H. & Tsien, R. Y. The fluorescent toolbox for assessing protein location and function. *Science* **312,** 217–224 (2006).
7. Rider, T. H. *et al.* AB cell-based sensor for rapid identification of pathogens. *Sci. Signal.* **301,** 213–215 (2003).

8. Fenno, L., Yizhar, O. & Deisseroth, K. The development and application of optogenetics. *Annu. Rev. Neurosci.* **34,** 389–412 (2011).
9. Ye, H., Daoud-El Baba, M., Peng, R. W. & Fussenegger, M. A synthetic optogenetic transcription device enhances blood-glucose homeostasis in mice. *Science* **332,** 1565–1568 (2011).
10. Wang, X., Chen, X. & Yang, Y. Spatiotemporal control of gene expression by a light-switchable transgene system. *Nature Methods* **9,** 266–269 (2012).
11. Toettcher, J. E., Gong, D., Lim, W. A. & Weiner, O. D. Light-based feedback for controlling intracellular signaling dynamics. *Nature Methods* **8,** 837–839 (2011).
12. Kim, M. *et al.* Maximal energy transport through disordered media with the implementation of transmission eigenchannels. *Nature Photon.* **6,** 583–587 (2012).
13. Kwon, K., Son, T., Lee, K. J. & Jung, B. Enhancement of light propagation depth in skin: cross-validation of mathematical modeling methods. *Lasers Med. Sci.* **24,** 605–615 (2009).
14. Sparta, D. R. *et al.* Construction of implantable optical fibers for long-term optogenetic manipulation of neural circuits. *Nature Protoc.* **7,** 12–23 (2012).
15. Zhao, S. *et al.* Cell type-specific channelrhodopsin-2 transgenic mice for optogenetic dissection of neural circuitry function. *Nature Methods* **8,** 745–752 (2011).
16. Hoffman, A. S. Hydrogels for biomedical applications. *Adv. Drug Deliv. Rev.* **54,** 3–12 (2002).
17. Jain, A., Yang, A. H. J. & Erickson, D. Gel-based optical waveguides with live cell encapsulation and integrated microfluidics. *Opt. Lett.* **37,** 1472–1474 (2012).
18. Wang, Y. *et al.* Biosensor based on hydrogel optical waveguide spectroscopy. *Biosens. Bioelectr.* **25,** 1663–1668 (2010).
19. Lee, S. C., Kwon, I. K. & Park, K. Hydrogels for delivery of bioactive agents: a historical perspective. *Adv. Drug Deliv. Rev.* **65,** 17–20 (2013).
20. Kloxin, A. M., Tibbitt, M. W. & Anseth, K. S. Synthesis of photodegradable hydrogels as dynamically tunable cell culture platforms. *Nature Protoc.* **5,** 1867–1887 (2010).
21. Tibbitt, M. W. & Anseth, K. S. Hydrogels as extracellular matrix mimics for 3D cell culture. *Biotechnol. Bioeng.* **103,** 655–663 (2009).
22. Lin, S., Sangaj, N., Razafiarison, T., Zhang, C. & Varghese, S. Influence of physical properties of biomaterials on cellular behavior. *Pharm. Res.* **28,** 1422–1430 (2011).
23. Choi, W. *et al.* Tomographic phase microscopy. *Nature Methods* **4,** 717–719 (2007).
24. Taniguchi, A. Live cell-based sensor cells. *Biomaterials* **31,** 5911–5915 (2010).
25. Drucker, D. J. Glucagon-like peptides. *Diabetes* **47,** 159–169 (1998).
26. Wang, Z. & Gleichmann, H. GLUT2 in pancreatic islets: crucial target molecule in diabetes induced with multiple low doses of streptozotocin in mice. *Diabetes* **47,** 50–56 (1998).
27. Parker, S. T. *et al.* Biocompatible silk printed optical waveguides. *Adv. Mater.* **21,** 2411–2415 (2009).
28. Dupuis, A. *et al.* Prospective for biodegradable microstructured optical fibers. *Opt. Lett.* **32,** 109–111 (2007).
29. Wu, Y.-H., Park, H. B., Kai, T., Freeman, B. D. & Kalika, D. S. Water uptake, transport and structure characterization in poly(ethylene glycol) diacrylate hydrogels. *J. Membr. Sci.* **347,** 197–208 (2010).
30. Yu, L. & Ding, J. Injectable hydrogels as unique biomedical materials. *Chem. Soc. Rev.* **37,** 1473–1481 (2008).
31. Slaughter, B. V., Khurshid, S. S., Fisher, O. Z., Khademhosseini, A. & Peppas, N. A. Hydrogels in regenerative medicine. *Adv. Mater.* **21,** 3307–3329 (2009).
32. Murua, A. *et al.* Cell microencapsulation technology: towards clinical application. *J. Control. Rel.* **132,** 76–83 (2008).
33. Wurm, F. M. Production of recombinant protein therapeutics in cultivated mammalian cells. *Nature Biotechnol.* **22,** 1393–1398 (2004).
34. Eyrich, D. *et al.* Long-term stable fibrin gels for cartilage engineering. *Biomaterials* **28,** 55–65 (2007).
35. Sharma, B. *et al.* Human cartilage repair with a photoreactive adhesive-hydrogel composite. *Sci. Transl. Med.* **5,** 167ra6 (2013).
36. Holtz, J. H. & Asher, S. A. Polymerized colloidal crystal hydrogel films as intelligent chemical sensing materials. *Nature* **389,** 829–832 (1997).
37. Ge, S., Zhang, C., Zhu, Y., Yu, J. & Zhang, S. BSA activated CdTe quantum dot nanosensor for antimony ion detection. *Analyst* **135,** 111–115 (2010).

Acknowledgements

The authors thank M. Fussenegger and H. Ye (ETH) for providing plasmids for optogenetic experiments. This work was funded by the US National Institutes of Health (R21 EB013761), the US National Science Foundation (ECS-1101947), the US Department of Defense (FA9550-10-1-0537), the IT Consilience Creative Program of MKE and NIPA (C1515-1121-0003) and the Bio & Medical Technology Development Program and the World Class University Program of the Korean National Research Foundation (2012M3A9C6049791 and R31-2008-000-10071-0). S.N. acknowledges financial support from the Bullock–Wellman Fellowship.

Author contributions

M.C. and S.H.Y. designed the experiments. M.C. performed the experiments. J.W.C., S.K. and S.N. provided materials. M.C., S.K., S.K.H. and S.H.Y. analysed the data. M.C. and S.H.Y. wrote the manuscript, with input from all authors.

Additional information

Supplementary information is available in the online version of the paper. Reprints and permissions information is available online at www.nature.com/reprints. Correspondence and requests for materials should be addressed to S.H.Y.

Competing financial interests

The authors declare no competing financial interests.

Supplementary Information

Light-guiding hydrogels for cell-based sensing and optogenetic synthesis *in vivo*

Myunghwan Choi[1,2], Jin Woo Choi[1,3], Seonghoon Kim[2], Sedat Nizamoglu[1], Sei Kwang Hahn[1,4], and Seok Hyun Yun[1,2]*

[1] Harvard Medical School and Wellman Center for Photomedicine, Massachusetts General Hospital, Boston, Massachusetts, USA.
[2] WCU Graduate School of Nanoscience and Technology, Korea Advanced Institute of Science and Technology, Daejeon, Korea.
[3] Wonkwang Institute of Interfused Biomedical Science, Department of Pharmacology, School of Dentistry, Wonkwang University, Seoul, Korea.
[4] Department of Materials Science and Engineering, Pohang University of Science and Technology, Pohang, Korea.

*Corresponding should be addressed to
S. H. Andy Yun, Ph.D.
Associate Professor
65 Landsdowne St. UP-525, Cambridge, MA 02139, USA
Email: syun@hms.harvard.edu

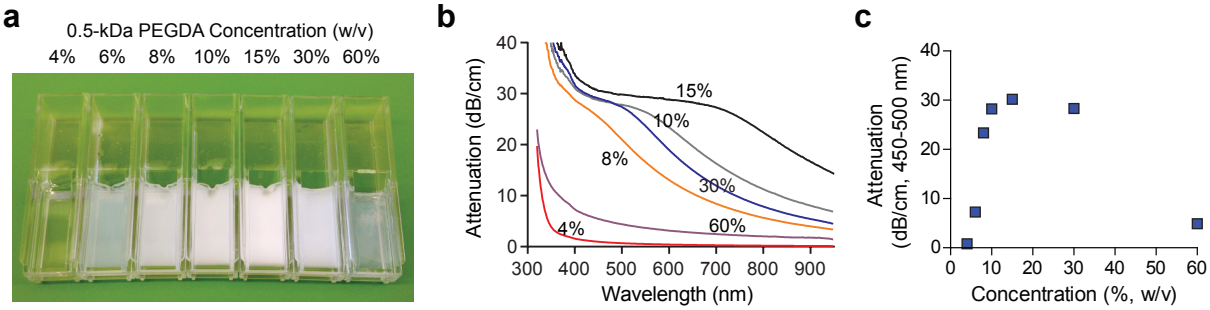

Supplementary Fig. S1 | Effect of the precursor concentration on optical transparency. (**a**) Photographs of PEG hydrogels at varying concentrations of PEGDA (0.5 kDa) in standard 1-cm-wide cuvettes. (**b**) Optical attenuation spectra. (**c**) Average attenuation coefficients averaged over a spectral range of 450-500 nm.

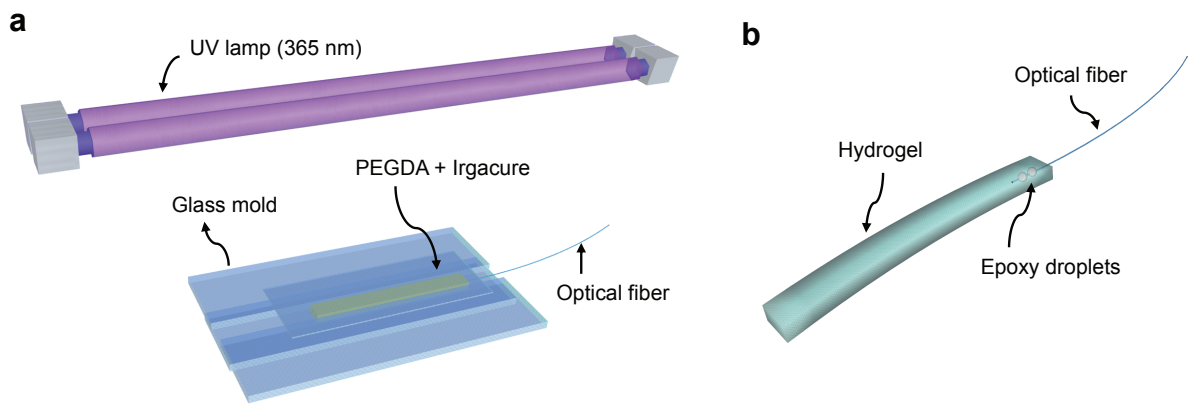

Supplementary Fig. S2 | Fabrication of a hydrogel optical waveguide. (**a**) Precursor solution containing PEG diacrylates (PEGDA) and photoinitiator (Irgacure) was photo-crosslinked *in situ* in a glass mold. (**b**) Schematic of the fabricated hydrogel optical waveguide.

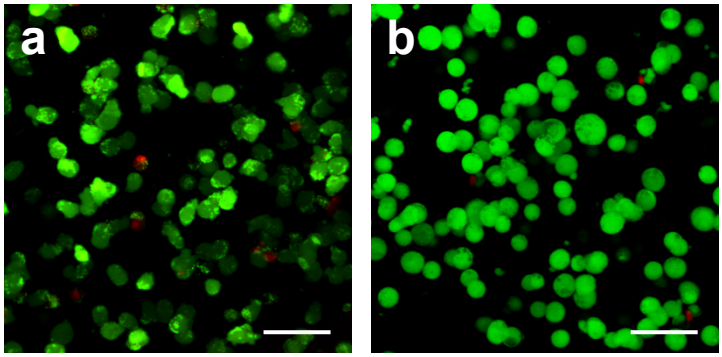

Supplementary Fig. S3 | Cell viability after hydrogel encapsulation. (**a**) HEK293 human embryonic kidney cell line. (**b**) EL4 mouse T cell line. Cells were encapsulated in PEG hydrogel through photopolymerization and cell viability was tested by staining with calcein AM (green; viable cells) and ethidium homodimer (red; dead cells). In the hydrogels, 96% of the HEK293 cells are live after encapsulation (a), and 97.5% of EL4 cells are live (b). Scale bar, 50 μm.

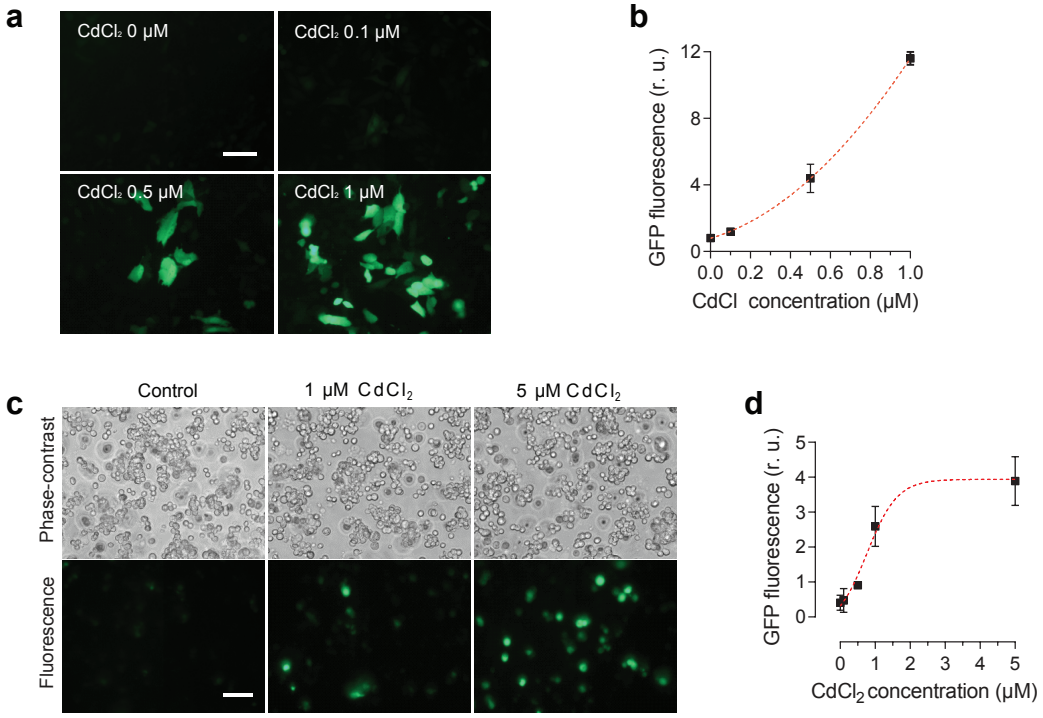

Supplementary Fig. S4 | Activation of heat-shock protein (hsp70) gene in response to cadmium ions. (**a**) Fluorescence images of the hsp-70-GFP sensing cells *in vitro*. (**b**) Dose-dependent activation of GFP fluorescence. (c) Phase contrast images and corresponding fluorescence images of the sensing cells in a hydrogel at 24 hours after $CdCl_2$ was added to the medium. (**d**) Dose-dependent activation of GFP signal *in vitro*.

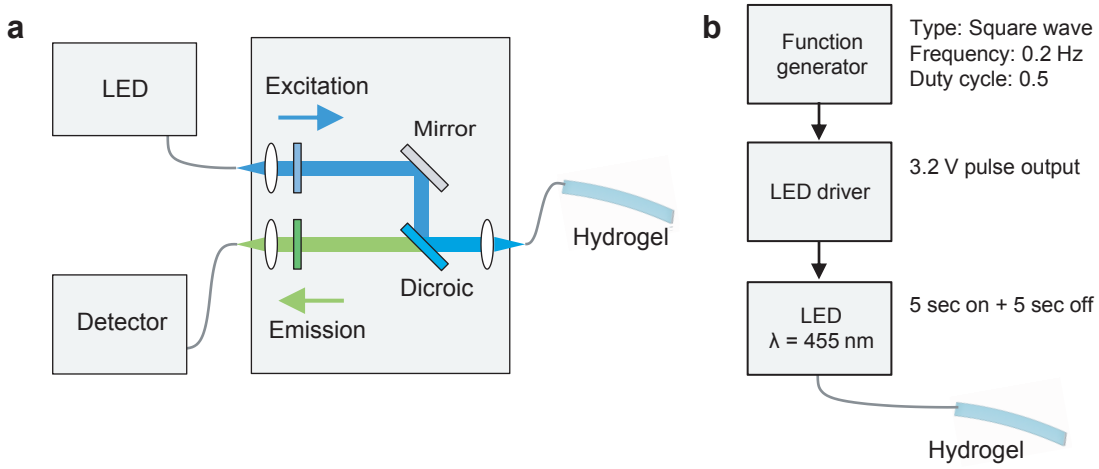

Supplementary Fig. S5 | Schematic of the experimental setups for sending and receiving light to and from a hydrogel. (**a**) Setup for fluorescence sensing. A fiber-coupled blue LED (λ = 455 nm; excitation) was coupled to the hydrogel through the pigtail fiber and the fluorescence emission (500-550 nm) was collected to a photo-detector. (**b**) Setup for optogenetic therapy. To generate pulsed blue light, a light emitting diode (LED) was driven in a pulsed mode at 0.1 Hz.

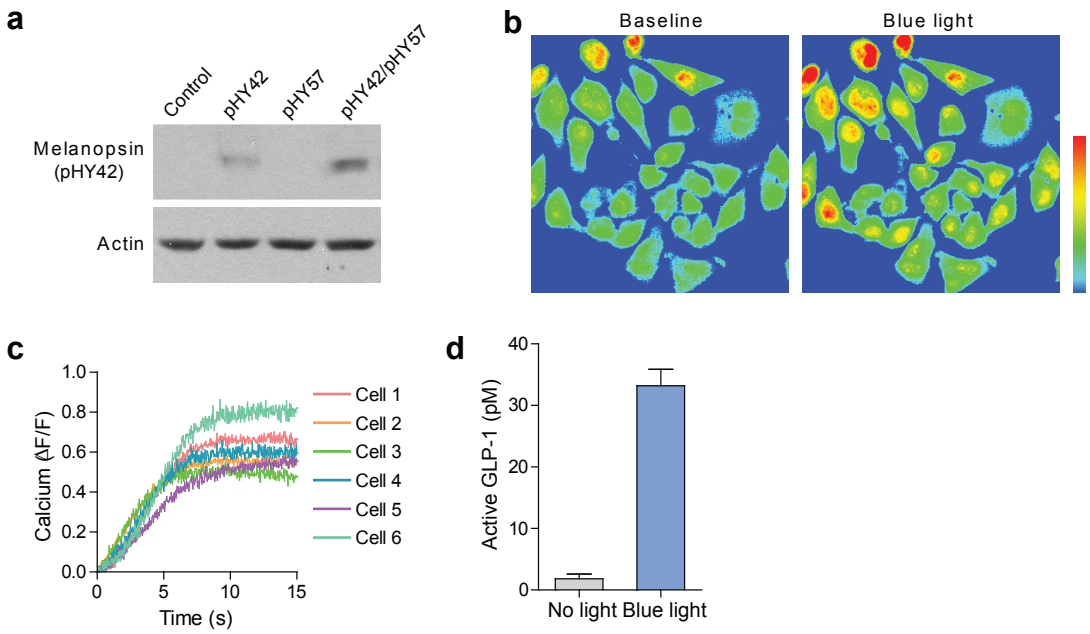

Supplementary Fig. S6 | Stable cell line for light-induced GLP-1 secretion, produced with two plasmids named pHY42 (human melanopsin) and pHY57 (NFAT promoter driven GLP-1 expression). (**a**) Western blot analysis confirming the expression of melanopsin. (**b**) Fluorescence calcium-level images before and after illuminating blue light (10 s). The cells were preloded with a fluorescent calcium indicator. (**c**) Time traces of the calcium signals in various cells. (**d**) The GLP-1 level in the cell media measured by ELISA before and after illuminating blue activation light.

Supplementary Video S1

A fully awake mouse with a hydrogel (4 mm x 1 mm x 40 mm) implanted in the subcutaneous pocket. Video was taken one day after implantation.